




# Enhancing the Air Conditioning Unit Performance via Energy Storage of Different Inorganic Phase Change Materials with Hybrid Nanoparticles

M. ISMAIL <sup>1,2,7</sup> W.K. ZAHRA,<sup>3,4</sup> SHINICHI OOKAWARA,<sup>1,5</sup>  
and HAMDY HASSAN<sup>1,6</sup>

1.—Energy Resources Engineering Department, Egypt-Japan University of Science and Technology (E-JUST), Alexandria, Egypt. 2.—Mechanical Engineering Department, Faculty of Engineering, Suez University, Suez, Egypt. 3.—Department of Mathematics, Institute of Basic and Applied Sciences, Egypt-Japan University of Science and Technology (E-JUST), Alexandria, Egypt. 4.—Department of Engineering Physics and Mathematics, Faculty of Engineering, Tanta University, Tanta, Egypt. 5.—Department of Chemical Science and Engineering, Tokyo Institute of Technology, Tokyo, Japan. 6.—Mechanical Engineering Department, Faculty of Engineering, Assiut University, Assiut, Egypt. 7.—e-mail: mohamed.abdelmawla@ejust.edu.eg

Air conditioning unit performance, coupled with new configurations of phase change material as thermal energy storage, is investigated in hot climates. During the daytime, the warm exterior air temperature is cooled when flowing over the phase change material structure that was previously solidified by the night ambient air. A theoretical transient model is constructed and solved numerically for the proposed design in plate and cylinder configurations. This model is studied at different inlet hot ambient air temperatures and phase change material types (SP24E and SP26E) without and with inclusion of hybrid nanoparticles. The results affirm that the discharging and charging duration for the cylinder is minimal compared to the plate configuration. Raising the inflow air temperature lowers the exit air temperature and air conditioning coefficient of performance and power-saving but shortens the cooling time. Using phase change material with a relatively low melting temperature increases the melting time and exit air temperature but reduces the charging time. Mixing hybrid nanoparticles with phase change material has a short-term positive influence on air conditioning performance. The maximum power saving for 2 h of working is 16.4% for the cylinder, while for 10 h of working, it is 6.4% for the plate.

## List of symbols

AC	Air conditioning	FCT	Full cooling time
COP	Coefficient of performance	FMT	Full melting time
$C_p$	Specific heat (J/kg K)	FST	Full solidification time
EAT	Exit air temperature	out	Outlet
$g$	Gravitational acceleration (m/s <sup>2</sup> )	$p$	Pressure (Pa)
$h$	Specific enthalpy (J/kg)	PCM	Phase change material
$H$	Total enthalpy (J)	$P$	Turbulence kinetic energy generation
HN	Hybrid nanoparticles	$Q$	Heat flux (W/m <sup>2</sup> )
in	Inlet	$S_i$	Damping coefficient of darcy's law
$k$	Thermal conductivity (W/m K)	$T$	Temperature (K)
$L$	Latent heat (J/kg)	$u$	Velocity (m/s)
$m$	Mass (kg)	$W$	Consumed power (W)
MT	Melting temperature	$\beta$	Melting fraction
		$\mu$	Dynamics viscosity (m/s <sup>2</sup> )
		$\rho$	Density (kg/m <sup>3</sup> )
		$\Delta H$	Latent heat content (J/kg)

(Received July 11, 2022; accepted November 27, 2022;  
published online January 3, 2023)

## INTRODUCTION

The proportional increase in demand for air conditioning (AC) and refrigeration systems follows the growth of the world's population and the development of urban areas. AC is essential for regulating the indoor environment in buildings so that residents can choose their desired temperature and achieve better air quality.<sup>1,2</sup> In this regard, researchers have made significant attempts to cut down on the energy consumption of AC systems. The coefficient of performance (COP) of AC systems could be enhanced by lower condenser temperature or higher evaporator temperature.<sup>3</sup> Increasing the on-coil condenser temperature by 1 degree causes a drop of 3% in the AC unit's COP.<sup>4</sup> Accordingly, minimizing the condenser's temperature leads to a considerable improvement in the COP of the AC unit and hence lowers the energy consumption. There are various methods to lower the temperature of AC condensers,<sup>5</sup> including alternative refrigerant types,<sup>6</sup> optimizing condenser positioning,<sup>7</sup> adopting a variety of condenser materials,<sup>8</sup> and analyzing the effect of temperature stacks.<sup>9</sup> The inclusion of thermal energy storage systems inside a building's AC system is one of the intriguing technologies that has lately attracted researchers to optimize and reduce energy consumption. Thermal energy storage of PCM is regarded as a feasible option for maximizing the use of cold energy during the night to reduce the amount of electricity consumed by AC units during the day.<sup>2</sup> PCM has a larger energy potential than other heat storage solutions since it tends on its phase transition to store heat over a specified temperature range.<sup>10,11</sup> Implementing low nighttime temperatures solidifies the PCM, which retains cold energy. This stored energy is utilized for daytime cooling the next day.

Building heating and cooling systems with PCM has been investigated in many studies.<sup>3,12–21</sup> Selvenes et al.<sup>21</sup> reviewed PCM's applications as thermal energy storage in multiple AC technologies. Also, they stated the top concerns to be considered in the future investigation of cold storage applications. Different approaches and techniques were reviewed and investigated by Vakiloroy et al.,<sup>14</sup> revealing their effect on the performance of HVAC systems while reducing power consumption. Souayfane et al.<sup>18</sup> presented a review article on the different aspects of PCMs that can be used in buildings to reduce the cooling demand in diverse environments. They mentioned the parameters that influence the PCM application's success and effectiveness. Jeon et al.<sup>19</sup> conducted a review article on the advancement of various latent heat TES systems. Moreover, they analyzed the application of PCM in buildings, such as ceiling heating technologies. A numerical investigation was conducted by Saffari et al.<sup>10</sup> to assess the most proper PCM discharging temperature in buildings. They recommended that

discharging temperatures of 26°C and 20°C are suitable for cooling and heating environments, respectively. Panchabikesan et al.<sup>22</sup> increased the free cooling capability by employing an alternative cooling method. A spherically encapsulated PCM and water spray nozzles were added to a cylindrical vessel's inlet. This mixed cooling technique lowered the solidification time by about 30% and enhanced the heat transfer rate. Said and Hassan<sup>2,23</sup> demonstrated experimental and numerical investigations on improving AC performance with TES. The basis of their investigation was connecting the PCM plates to the AC unit to cool down the outside air. They concluded that the AC unit using PCM plates performs better in terms of COP than the one not using them. An HVAC PCM pack integration study was conducted by Ajour et al.<sup>24</sup> According to their findings, both electricity usage and carbon dioxide emissions decreased. Hai et al.<sup>25</sup> simulated the impact of integrating PCM cylinders in a building's AC system. Their research compared PCM's summer night discharging procedure with different cylinder diameters, inflow temperatures, and Reynolds numbers. According to their findings, raising the cylinders' diameter or lowering the Reynolds number speeds up PCM discharging. Hoseini et al.<sup>26</sup> analyzed the AC system through two-hybrid methods, ice TES and PCM. The result showed that using PCM and ice TES decreased the power consumption by 7.58% and 4.59%, respectively, compared to the traditional system. Furthermore, PCM and ice systems produced 17.8% and 27.2%, respectively, less CO<sub>2</sub> than the traditional one. Said and Hassan<sup>27</sup> simulated the effect of using various PCM types (24 E, 26 E, and 29 Eu) on the AC system's performance. Results demonstrated that the power consumption of the AC system coupled with PCM was lowered maximally by about 8.95% in the case of PCM 29 Eu. Huang et al.<sup>28</sup> tested the integration of PCM with roof ACS in a data center room during emergency cooling. They found that the PCM provided the necessary emergency conditioning for periods of 300 s and 900 s. To discover strategies to reduce ACS's energy consumption, Muzhanje et al.<sup>29</sup> analyzed the results of theoretical and experimental investigations of PCM applications. Based on the results of their analysis, they assessed that coupling PCM with ACS boosted COP by 1.8% and decreased power by at least 5%.

Most current PCMs exhibit low thermal conductivity, resulting in a reduced heat transfer in implementations of PCM with AC systems. Thus, numerous types of research were conducted to enhance the PCM thermal conductivity by mixing it with superior thermal conductivity nanoparticles.<sup>30–36</sup> A comprehensive review of the current progressions of nano-enhanced PCM was carried out by Muzhanje et al.<sup>5</sup> and Yang et al.<sup>37</sup> They presented the different preparation methods of this mixture as well as their effectiveness and applications. Parameshwaran and Kalaiselvam<sup>32</sup> improved

the thermal characteristics of a chilled-water AC unit by integrating a silver nanoparticle-embedded PCM system experimentally. On-peak power savings of around 24% were achieved by the modified AC system compared to the traditional one, according to the results of the experiments. A numerical study was carried out by Karunesh et al.<sup>33</sup> exploring the discharging process of PCM mixed with graphene nanoparticles inside an aluminum tank. The results affirmed that the inclusion of graphene nanoparticles boosted the discharging process of the PCM. Sun et al.<sup>36</sup> investigated the change of thermal-physical characteristics of PCM enhanced with nano-carbons. The discharging time of the mixture was decreased by 21% when using 0.06 wt.% nano-carbons, according to their experimental findings. The effect of utilizing hybrid nanoparticles on the charging rate of PCM was studied by Hosseinzadeh et al.<sup>38</sup> Their numerical results revealed that applying hybrid nanoparticles considerably enhanced the PCM charging rate.

Integrating PCM-based TES with AC systems has been shown to boost AC system performance, as revealed in previous research. As far as the authors found, only few works have investigated that the direct connection of the PCM heat exchanger to the AC condenser could improve the performance of the AC. In addition, the majority of earlier works only utilized PCM encased in plates for the PCM heat exchanger.<sup>2,27</sup> A key drawback is that PCM plates require a long time to solidify; thus, they cannot be fully charged overnight. This makes them impractical for daily use in AC systems. To this point, this research conceptually utilizes previously unstudied configurations (inline tube bank) of the PCM container to examine their impact on the PCM solidification and melting process and the AC system's efficiency. Using the same conditions, the optimal PCM plate arrangement from previous studies is retested and compared to the aforementioned configurations based on PCM and AC performance. In addition, as was previously indicated, the addition of nanoparticles to PCM resulted in a promising improvement in thermal conductivity. Consequently, the effect of combining nanoparticles of remarkably high thermal conductivity impeded within the PCM on the AC system performance is evaluated.

Furthermore, commercial phase change materials, including PCM SP24E and PCM SP26E, are utilized to determine their impact on the performance of the modified AC unit. A complete theoretical transient model of the physical model is constructed and solved numerically by ANSYS software for the proposed design of the different configurations. Through this model, it is possible to estimate the EAT and liquid fraction of PCM with the variation of inlet hot ambient air temperature, air speed, and PCM type. The impact of these parameters on the AC unit's COP and power usage is presented.

## PHYSICAL MODEL

The theoretical model was created to numerically analyze the performance of the thermal energy storage unit based on an air-PCM heat exchanger coupled with an AC unit. The proposed model consists of PCM, with two different configurations, embedded in a rectangular duct through which air flows, as shown in Fig. 1. Both structures have the same PCM volume, and their geometry and dimensions are illustrated in Fig. 2 and Table I. The commercially available PCM SP24E (PCM-24) and PCM SP26E (PCM-26) from Rubitherm were employed in this investigation<sup>2,27</sup> because of their small volume expansion during the discharging process and range of temperature acceptable for air conditioners, night temperature for solidification and day temperature for condenser cooling. Table II illustrates the used PCM properties. To promote the thermal conductivity of the PCM, solid Cu and Al<sub>2</sub>O<sub>3</sub> nanoparticles with a total concentration ratio of 5% are combined with the used PCMs to produce hybrid nano-enhanced PCM-24 (HNPCM-24) and hybrid nano-enhanced PCM-26 (HNPCM-26). The specifications of these nanoparticles are presented in Table III. The chilly outdoor air flows through the PCM during the night, whereas the charging process is carried out. Discharging PCM cools the hot outdoor air the next day.

## Governing Equations

In this investigation, ANSYS software is used to create a two-dimensional dynamic model that includes both air and PCM as heat transfer media. The change in phase of the PCM and the air flow is regarded as transient, incompressible, and turbulent. The ANSYS melting-solidification model is used to simulate the phase transition of PCM. Dependent on the quantity of liquid fraction, this model employs the enthalpy-porosity approach to determine whether a liquid or solid phase is present. In addition, the PCM and nanoparticles are assumed to act as a homogeneous mixture in thermo-dynamic equilibrium, with no velocity slip between the two systems. The Boussinesq method is applied to evaluate the difference in PCM density to apply the bouncing thermal impact in the melted PCM, which results in free convection currents. The influences of melting volume expansion, terminal effects, and heat radiation are negligible. Air flow characteristics, heat transfer between air and PCM, air temperature variation, and PCM melting process are obtained by combining continuity, Navier-Stokes, energy, and phase transition equations with AC unit model equations. This model includes viscous energy dissipation. Governing continuity, momentum, and energy equations are as follows:<sup>40</sup>

Continuity,

$$\frac{\partial \rho}{\partial t} + \nabla \cdot (\rho u_i) = 0 \quad (1)$$

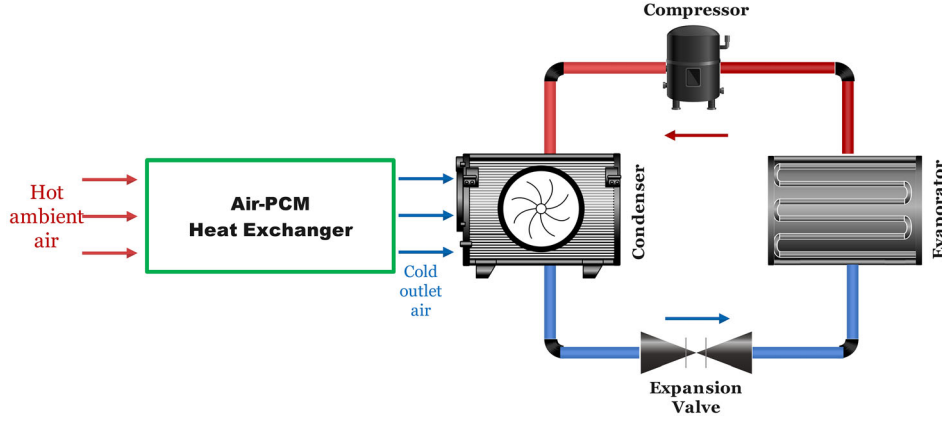


Fig. 1. Proposed model of air-PCM heat exchanger coupled with AC unit.

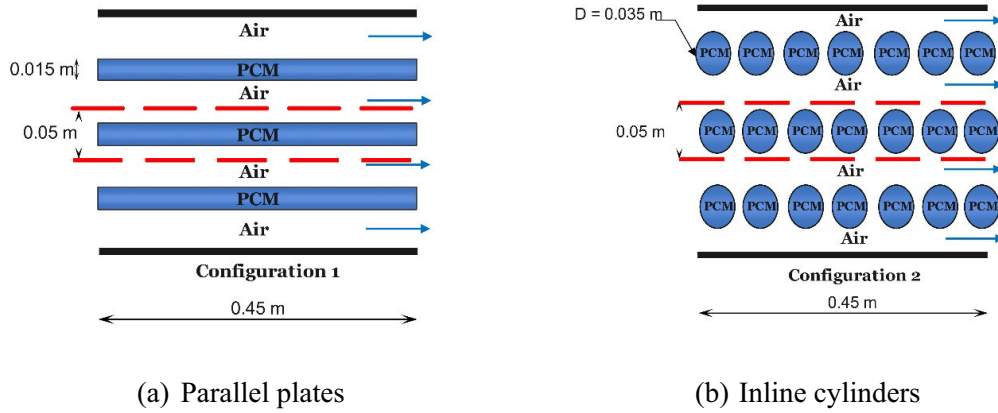


Fig. 2. Configurations of air-PCM heat exchanger: (a) parallel plates and (b) inline cylinders.

Table I. PCM configuration specification

Configuration	Cases	Number per each row ( $N$ )	Dimensions	Cross-sectional area ( $m^2$ )
Cylinders	Inline tube bank (CYL)	7	$D = 0.035$ m	0.006735
Plates	Horizontal plates (PL)	1	Rectangular (0.45 m $\times$ 0.015 m)	0.00675

Momentum,

$$\frac{\partial(\rho u)}{\partial t} + \partial_j(\rho u_i u_j) = \mu \partial_{jj} u_i - \partial_i p + \rho g_i + S_i \quad (2)$$

Energy,

$$\frac{\partial(\rho H)}{\partial t} + \partial_i(\rho u_i H) = \partial_i(K \partial_i T) \quad (3)$$

where  $S_i$  is the phase-changing impact on the convection of the PCM domain. This term is expressed as:<sup>40</sup>

$$S_i = \frac{C(1-\beta)^2}{\beta^3} u_i \quad (4)$$

where  $C$  represents the mushy zone constant. The total enthalpy ( $H$ ):<sup>40</sup>

$$H = \Delta H + h \quad (5)$$

where sensible heat ( $h$ ):

$$h = h_{\text{ref}} + \int C_p dT \quad (6)$$



**Table II. PCM properties<sup>27</sup>**

Properties	PCM SP24E (PCM-24)	PCM SP26E (PCM-26)
Melting range (K)	297–298	299–300
$\rho_{\text{liquid}}$ (kg/m <sup>3</sup> )	1400	1400
$\rho_{\text{solid}}$ (kg/m <sup>3</sup> )	1500	1500
Kinematic viscosity (m <sup>2</sup> /s)	0.1111	0.1111
Specific heat (J/kg K)	2000	2000
Thermal conductivity (W/m K)	0.6	0.6
Latent heat of fusion (kJ/kg)	180	180
Volume expansion (%)	6	5
Maximum operating temperature (K)	318	318

**Table III. Properties of used nanoparticles<sup>39</sup>**

Properties	Cu	Al <sub>2</sub> O <sub>3</sub>
Density kg/m <sup>3</sup>	401	40
Thermal conductivity (W/m K)	8933	3970
Specific heat (J/kg K)	386	765

**Table IV.  $C_1$  and  $C_2$  values<sup>2,40</sup>**

$T_r$ (K)	$C_1$	$C_2$
296	4.825	0.0687
298	5.153	0.0738
300	5.241	0.074

while PCM's latent heat ( $\Delta H$ ) is  $L$  for liquid and zero for solid.

The melt fraction  $\beta$  is addressed as:<sup>41,42</sup>

$$\beta = \begin{cases} \frac{\Delta H}{L} = 0 & \text{if } T < T_s \\ \frac{\Delta H}{L} = 1 & \text{if } T > T_s \\ \frac{\Delta H}{L} = \frac{T - T_s}{T_1 - T_s} & \text{if } T_s < T_1 < T_s \end{cases} \quad (7)$$

Hence, the latent heat can be expressed as:<sup>40</sup>

$$\Delta H = \beta L \quad (8)$$

Standard  $K$ - $\epsilon$  turbulence models are solved to obtain the time scale and turbulent length.<sup>43,44</sup>

$$\frac{\partial(\rho K)}{\partial t} + \frac{\partial}{\partial x_i}(\rho k u_i) = \frac{\partial}{\partial x_i} \left[ \left( \mu + \frac{\mu_t}{\sigma_k} \right) \frac{\partial k}{\partial x_j} \right] + P_k + P_b - \rho - Y_M + S_k \quad (9)$$

$$\frac{\partial(\rho \epsilon)}{\partial t} + \frac{\partial}{\partial x_i}(\rho \epsilon u_i) = \frac{\partial}{\partial x_i} \left[ \left( \mu + \frac{\mu_t}{\sigma_\epsilon} \right) \frac{\partial \epsilon}{\partial x_j} \right] + C_{1e} \frac{\epsilon}{k} (P_k + C_{3e} P_b) - C_{2e} \rho \frac{\epsilon^2}{k} + S_\epsilon \quad (10)$$

$P_k$  and  $P_b$  are the generations of turbulence kinetic energy caused by the mean velocity variations and buoyancy, respectively.  $S_k$  and  $S_\epsilon$  are user-defined source terms.  $\sigma_k$  and  $\sigma_\epsilon$  represent the turbulent Prandtl numbers for  $K$  and  $\epsilon$ , respectively.  $Y_M$  means how much the fluctuating dilation in the compressible turbulence adds to the total rate of dissipation.  $C_{1e}$ ,  $C_{2e}$ , and  $C_{3e}$  are constants.

Heat transfer to PCM for time step (i) is obtained from:

$$Q_i = m_i c_p (T_{\text{in},i} - T_{\text{out},i}) = \rho u_i A c_p (T_{\text{in},i} - T_{\text{out},i}) \quad (11)$$

COP is widely used to estimate the AC unit's performance. For AC units, COP can be calculated at a given interior and exterior room temperature based on the manufacturer's data as follows:<sup>40,45</sup>

$$\text{COP} = C_1 - C_2 T_c \quad (12)$$

where  $C_1$  and  $C_2$  are constants and are dependent on the interior room temperature  $T_r$  as presented in Table IV and  $T_c$  is the exterior temperature prior to the condenser.

The power consumption ( $W$ ) is calculated as follows:

$$W = \frac{Q}{\text{COP}} \quad (13)$$

The simple theoretical analysis of inclusion is used to evaluate the hybrid nano-PCM density, dynamic viscosity, latent heat of fusion, specific capacity, and thermal conductivity as follows:<sup>30,38,39</sup>

$$\rho_{\text{HNPCM}} = \rho_{\text{PCM}} (1 - \varphi_{N2}) \left[ (1 - \varphi_{N1}) + \varphi_{N1} \left( \frac{\rho_{N1}}{\rho_{\text{PCM}}} \right) \right] + (\varphi \rho)_{N2} \quad (14)$$

$$\mu_{\text{HNPCM}} = 0.983 e^{12.958\varphi} \quad (15)$$

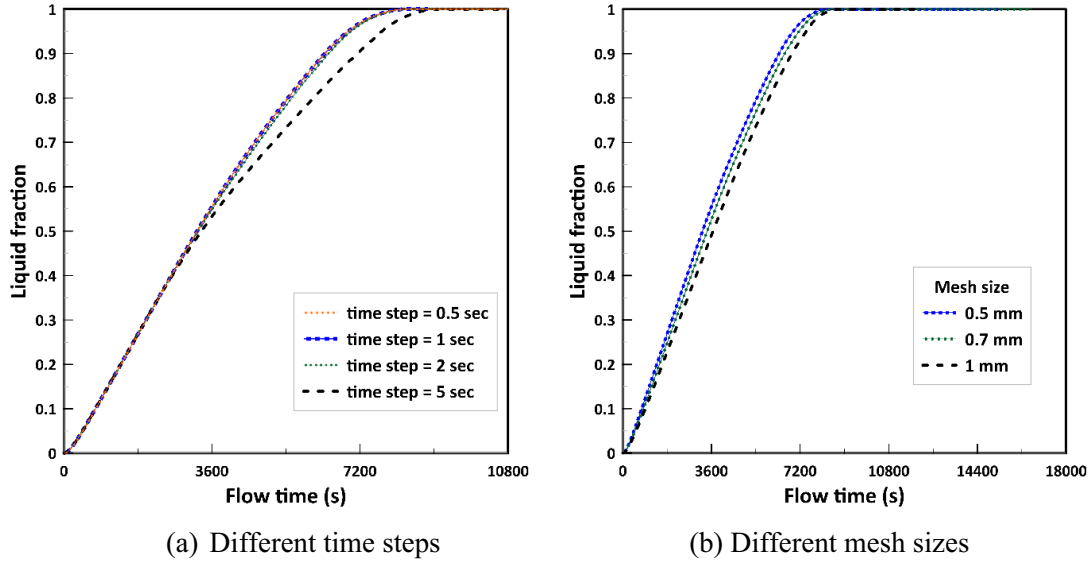


Fig. 3. Time variation of the liquid fraction at different (a) time steps and (b) mesh sizes.

$$L_{\text{HNPCM}} = \frac{(\rho L)_{\text{PCM}}(1 - \varphi_{N1})(1 - \varphi_{N2})}{\rho_{\text{HNPCM}}} \quad (16)$$

$$(\rho C_p)_{\text{HNPCM}} = (\rho C_p)_{\text{PCM}}(1 - \varphi_{N2}) \left[ (1 - \varphi_{N1}) + \varphi_{N1} \left( \frac{(\rho C_p)_{N1}}{(\rho C_p)_{\text{PCM}}} \right) \right] + (\varphi \rho C_p)_{N2} \quad (17)$$

$$\frac{K_{\text{HNPCM}}}{K_{\text{bf}}} = \frac{K_{N2} + 2K_{\text{bf}} - 2\varphi_{N2}(K_{\text{bf}} - K_{N2})}{K_{N2} + 2K_{\text{bf}} + \varphi_{N2}(K_{\text{bf}} - K_{N2})}, \quad (18)$$

$$\frac{K_{\text{bf}}}{K_{\text{PCM}}} = \frac{K_{N1} + 2K_{\text{PCM}} - 2\varphi_{N1}(K_{\text{PCM}} - K_{N1})}{K_{N1} + 2K_{\text{PCM}} + \varphi_{N1}(K_{\text{PCM}} - K_{N1})}$$

where  $\varphi$  is the nanoparticle's concentration ratio within PCM. The subscripts HNPCM, N, and bf represent hybrid nano-PCM, nanoparticles, and base fluid, respectively.

### Initial and Boundary Conditions

At first, the PCM is assumed to be solid at 295 K, below the PCMs melting point. Moreover, the no-slip boundary condition is considered the walls' boundary condition. Furthermore, the boundaries of the heat exchanger are assumed to be adiabatic. The volume flow rate of inflow air is regarded as constant (42 L/s) per unit width, which is adequate for the ACS fan power.<sup>2</sup> The study's ambient temperatures (308 K and 313 K) are chosen to suit the general weather conditions during day and night times in Egypt and several regions in the Middle East with an equivalent environment. Hence, the inflow air temperatures of the PCM system are 308 K and 313 K during discharging (daytime) and 295 K throughout charging

(nighttime). The pressure outlet with zero-gauge pressure is addressed as the heat exchanger's output boundary condition.

### COMPUTATIONAL METHODOLOGY

The equations of mass, energy, and momentum are solved using ANSYS software's finite volume approach. The PISO algorithm is adopted with the fully implicit method for unsteady simulation. The convective terms are approximated using a second-order upwind approach, and the k- $\epsilon$  model is employed to analyze the airflow and phase change disturbance. The Ansys fluent 2020 R2 software is used to solve the conservation equations to estimate the solution's temperature, velocity, and pressure for the investigation domain. Moreover, the pressure correction equation is corrected using the PRESTO approach.

### Time and Mesh Independent Test

Independent time and mesh tests are created to obtain the optimum time step and element size for the numerical solution validity and calculation time. Figure 3a and b reveals how the outcomes (liquid fraction) for CYL\_PCM-24 configuration are affected by the time step and mesh size, respectively. As shown, a 1-s time step and 0.5-mm element size are established to be adequate for the proposed model.

### Validation

Considering experimental data from Said and Hassan<sup>2</sup> on PCM plates with varying inlet temperatures, the computational solution of the model was validated. Figure 4 shows the experimental and current model results for modifying the EAT over time at varying input air temperatures. As shown,

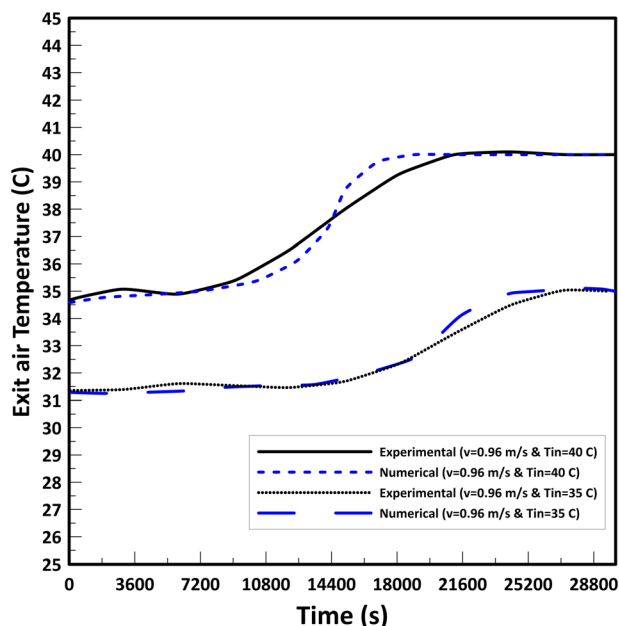


Fig. 4. Comparison of the current model results with experimental data of Said and Hassan.<sup>2</sup>

the maximum error between EAT's numerical and experimental results is approximately 4% for the analyzed situations.

## RESULTS AND DISCUSSION

The results of this study, as stated before, are conducted for two inflow air temperatures of 308 K and 313 K at an airflow rate of 42 L/s per unit width of the air-PCM heat exchanger. PCM container configurations are examined under these conditions, seven inline cylinders (CYL) and plates (PL) for two different PCMs with and without hybrid nano; PCM-24, HNPCM-24, PCM-26, and HNPCM-26. During the night, the PCM is given a charge of a cold temperature, which is required for solidification. During the day, the solid PCM is utilized to cool the ambient air during the process of discharging it (melting). It should be mentioned that while using PCM thermal storage for AC systems, two performance aspects could be taken into consideration: (1) air exit temperature when the melting process is taking place and (2) melting time (discharging). The first factor considerably impacts the COP of the air conditioner since lowering air exit temperature results in a lower condensing temperature and, as a result, improved efficiency. The duration of the PCM thermal storage capacity's potential for successful operation is determined, in part, by the second factor.

### Temperature and Melting Distribution

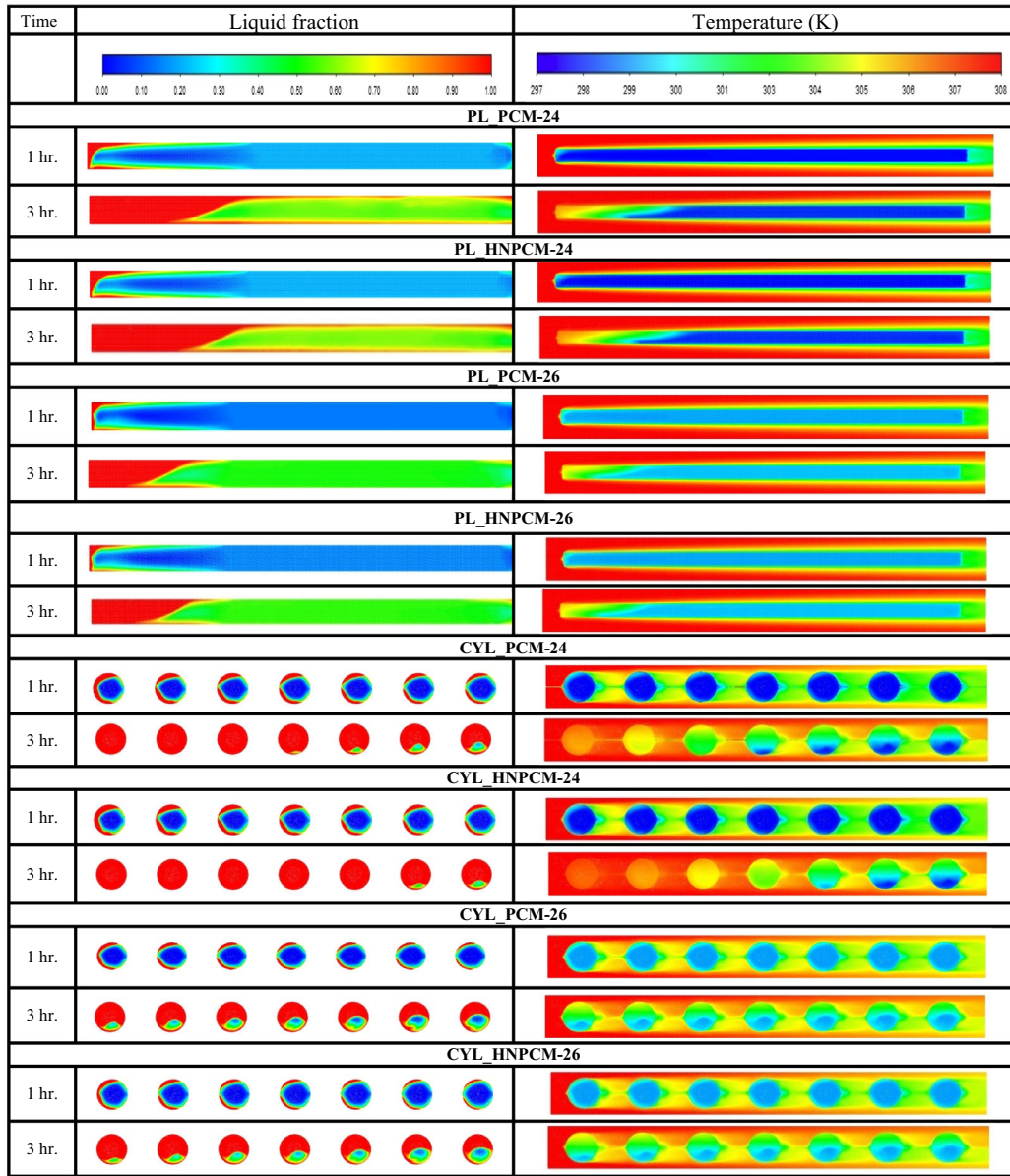
Figure 5 illustrates the distribution of the temperature and melting fraction of PCMs (with and without hybrid nano) for both configurations at different running times and inflow air

temperatures. Figure 5a shows the inflow temperature for 308 K and Fig. 5b for 313 K. With increasing air inflow temperature, the melting fraction and temperature of PCM increase. The same observation is noted by advancing in time. Different factors influence PCM melting, air-to-PCM heat transfer, and internal PCM heat transfer. In the beginning, only pure heat conduction occurs between the interior PCM and the hot PCM surfaces. As time passes, the PCM starts to melt, which increases the quantity of liquid PCM. During this period, free convection occurs in the liquid PCM, especially between solid PCM and walls, increasing the discharging rate at the surface of the solid PCM. Consequently, the air thermal boundary layer expands along with the PCM's surface, and the temperature difference between airflow and the PCM's surface reduces as a result. This influence increases until convection dominates at total PCM melting. Moreover, the high-temperature difference between the inflow air and the PCM at the start of the process results in a relatively great heat transfer. With advancing time, the heat transfer decreases as the PCM's temperature increases. Furthermore, the PCM's configuration affects the air-PCM heat transfer and melting processes. The temperature distribution findings affirm that turbulence occurs in the melty zone of the PCM within the solid zone, particularly at greater inflow air temperature, implying that convection within this area is enhanced (Fig. 5).

Mixing nanoparticles into the PCM causes the fluid's thermal conductivity to increase, slightly impacting heat transfer in the PCM, especially in the beginning. This leads to a relatively high melting rate compared to PCM only. Comparing the results of used PCMs, the discharging rate slows down, and the EAT rises when using PCM with higher MT. By comparing the liquid fraction of the different PCM configurations, the CYL configuration records the highest melting rate, while the PL configuration has the lowest melting rate for all studied cases under the same conditions, as will be seen later. This is because the cylinders provide an enhanced heat transfer rate compared to plates. Figure 5 shows the turbulent flow in the case of PL configuration at 313 K, Fig. 5b at 3 h, especially for HN-PCM-26.

### Variation of Melting Fraction

The time variation of the PCMs charging process (melting) is given in Fig. 6 for both configurations at two different inflow air temperatures: 308 K (Fig. 6a) and 313 K (Fig. 6b). The figures also present the effect of adding hybrid nanoparticles with PCMs on the melting fraction. The same trend of the melting fraction is obtained in both cases, where the liquid fraction rises with time from zero until complete melting (melting fraction equal 1) as expected. However, the higher the inflow air temperature,



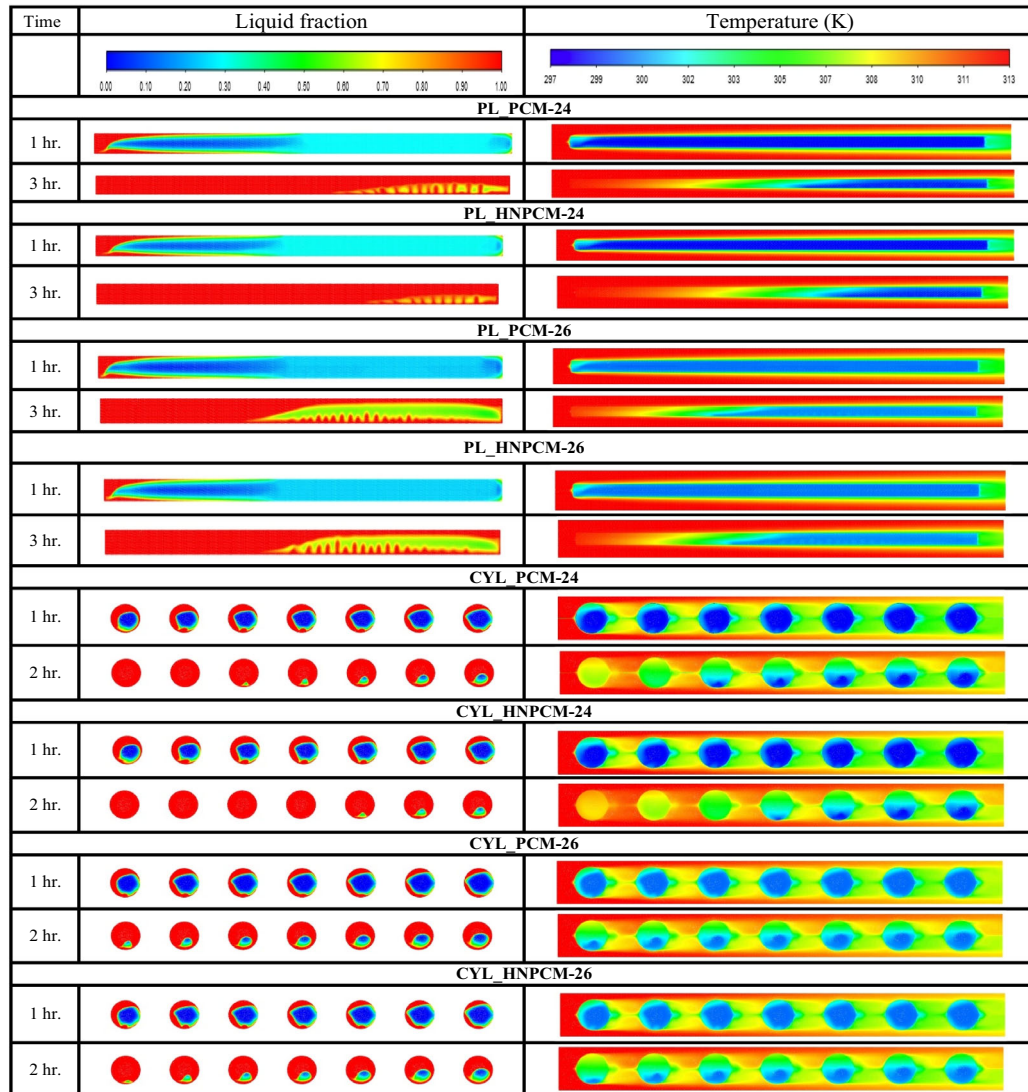
a) 308 K

Fig. 5. Liquid fraction and temperature distribution contours during PCM discharging after different processing times at inflow air temperatures of (a) 308 K and (b) 313 K.

the higher the curves' slopes are obtained. In other words, the melting time, for all cases, is shortened with the increase of inflow air temperature. This is due to increased heat transfer between the PCM and hot air with rising air flow temperature. The term "full melting time" refers to the length of time that the PCM takes to melt completely (FMT). The FMT in the case of 308 K is less than that of 313 K by about 1.5 h and 1 h for plate and cylinder configurations, respectively.

On the other hand, regarding the configurations, using cylinders resulted in faster melting than did plates, as noticed previously. In addition, the increase in PCM's melting temperature, from 24 to 26, delays the melting time for both cylinders and plates. Consequently, at 308 K, the FMT in the case of PCM-26 is higher by 0.75 h and 1.05 h than that in the case of PCM-24 for cylinders and plates, respectively, whereas the delayed times were 0.4 h and 0.5 h for the same order at 313 K. Moreover, it





b) 313 K

Fig. 5. continued.

is obvious that the addition of hybrid nanomaterials has a slight influence on the charging process time, where it decreases the melting time with about the same impact in all studied cases. On the basis of these findings, it can be concluded that the heat transfer rates are better in the case of cylinders than plates. Besides, the higher the PCM's MT, the lower the heat transfer that occurs, and accordingly, the discharging time increases. Finally, the hybrid nanomaterials slightly boost the PCM thermo-physical properties, resulting in a slightly rapid in charging process.

### Variation of Exit Air Temperature

As previously stated, lowering the air temperature near the condenser of an AC unit increases the unit's overall performance. The EAT from the air-

PCM heat exchanger is presented in Fig. 7 for various inflow air temperatures and PCMs. Besides, Table V lists PCM setups' FMT and full cooling time (FCT) for all analyzed cases. The FCT is the time elapsed from the PCM's initial start to its entire cooling (outlet air temperature is the same as the inlet). First, a sudden drop in the EAT is noticed because of the higher impact of the PCM cooling. This is followed by a rising tendency in the exit temperature over time. This is because heat transmission from cold solid PCM to warm air reduces because PCM's temperature gradually increases as it melts. Entrance and exit air temperatures will be equal after an elapsed time greater than the full PCM's melting time. At this point, all of the PCM material's cold energy is released (FCT). The results also reveal that the air temperature difference

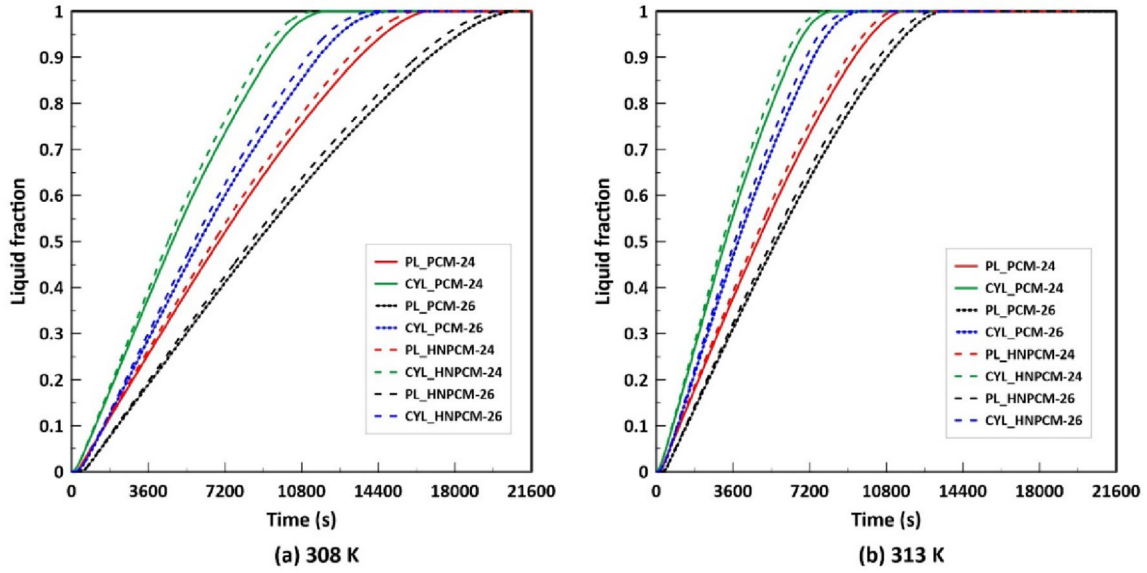


Fig. 6. Time variation of melting fraction at inflow air temperatures of (a) 308 K and (b) 313 K.

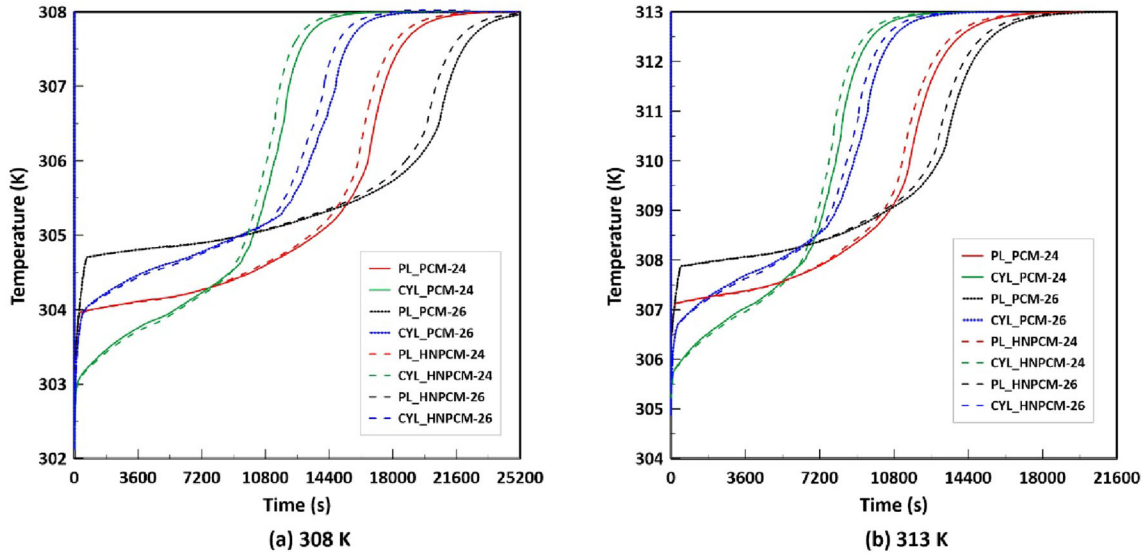


Fig. 7. Time variation of exit air temperature at inflow temperatures of (a) 308 K and (b) 313 K.

Table V. FMT and FCT of PCM configurations for all studied cases (hours)

Temperature	Configuration	PCM-24		HNPCM-24		PCM-26		HNPCM-26	
		FMT	FCT	FMT	FCT	FMT	FCT	FMT	FCT
308 K	CYL	3.25	4.5	3.15	4.25	4	5.2	3.75	5
	PL	4.7	6.35	4.4	6.2	5.75	7	5.5	6.8
313 K	CYL	2.25	3.8	2.2	3.6	2.65	4.1	2.5	3.9
	PL	3.2	5.1	3	4.8	3.7	5.6	3.5	5.4

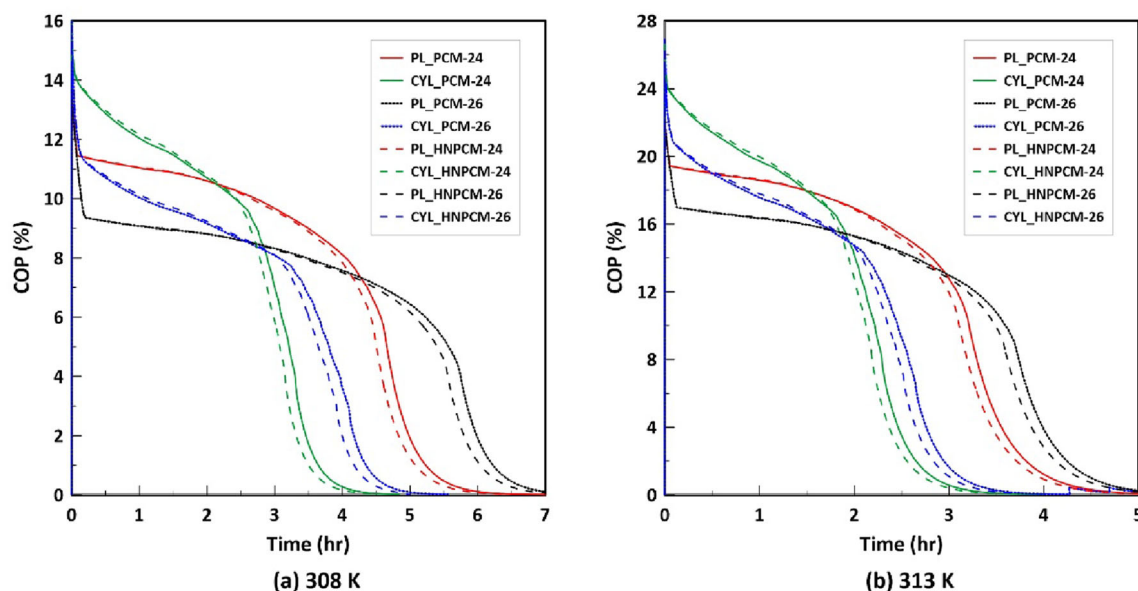


Fig. 8. Percentage enhancement of COP at inflow temperatures of (a) 308 K and (b) 313 K.

through the air-PCM heat exchanger rises with increasing inflow air temperature for all cases.

Regarding configurations, the initial EAT from the heat exchanger is lower for the CYL than that of the PL in all tests studied; however, the pattern reverses after a certain time. This implies that the rate of air-PCM heat transfer for CYL is greater at the beginning and subsequently reverses as the PCM temperature rises. Moreover, integrating nanoparticles into PCM reduces the EAT at the beginning before it rises after the complete melting of PCM. This is because the nano-PCM mixture has higher thermal properties than PCM only, as mentioned before, which raises the heat transfer inside the PCM. However, after melting the PCM, the impact of higher viscosity of the PCM with nanoparticles compared to PCM only reduces the heat transfer inside the PCM and hence to the flowing air. Figure 7 shows that nanoparticles have a small impact on the trend and melting time of the PCM. Furthermore, utilizing PCM with a higher MT increases the EAT at the beginning as it lowers the discharging rate. At 313 K, CYL\_HNPCM-24 has the greatest inlet-exit temperature difference, with a 7.5 K difference, while at 308 K, the PL\_HNPCM-26 exhibits the lowest inlet-exit temperature difference (around 3.5 K). These differences begin to disappear at the end of the cooling time for PCM. By analyzing the FCT of all studied cases, it is noted that the FCT of the cylinders with HNPCM-24 configuration at 313 K records the minimum value for multiple reasons: better heat transfer rate, maximum air-PCM temperature difference, and a lower PCM MT. In contrast, the PL with PCM-26 configuration has the longest FCT among all tested cases. The PCM cylinders give a better cooling rate in a short working period,

Compared to PCM plates. The maximum overall cooling time that PCM can work effectively is achieved using PCM-26, 7 h for PL and 5.2 h for CYL (Table V).

According to the foregoing findings, several parameters, such as the temperature of the entrance air and PCM setup, mixing nanoparticles, and the type of PCM, may be varied to govern FCT or the temperature of the air exiting the PCM heat exchanger at any specified time. Changing the PCM configuration and PCM type is significantly simpler and less costly than altering the input air temperature, which is governed by the ambient temperature. Thus, the optimal PCM configuration depends on the duration of the AC unit's operation; plates with PCM-26 are preferable for long-running units, while cylinders with HNPCM-24 are the best option for short-running units, as will be seen later.

## COP

The COP of an AC system is a crucial determinant of its effectiveness. It can be obtained from Eq. 13. Figure 8 illustrates the percentage gain with time in COP of the enhanced AC unit over the traditional unit for both configurations at various PCM types (without and with hybrid nano) at inflow air temperatures of 308 K and 313 K. At the start, the enhanced unit's COP is at its highest due to the abrupt EAT drops from the heat exchanger. Later, as time passes, it declines because EAT rises, as mentioned previously. The traditional and enhanced units both end up with the same COP at the end of the FCT that PCM can deliver. Analyzing Fig. 8a and b, the proportional gain in COP of the enhanced unit increases as the inflow air temperature rises. For instance, increasing inflow air temperature by 5 K leads to an initial rise in the

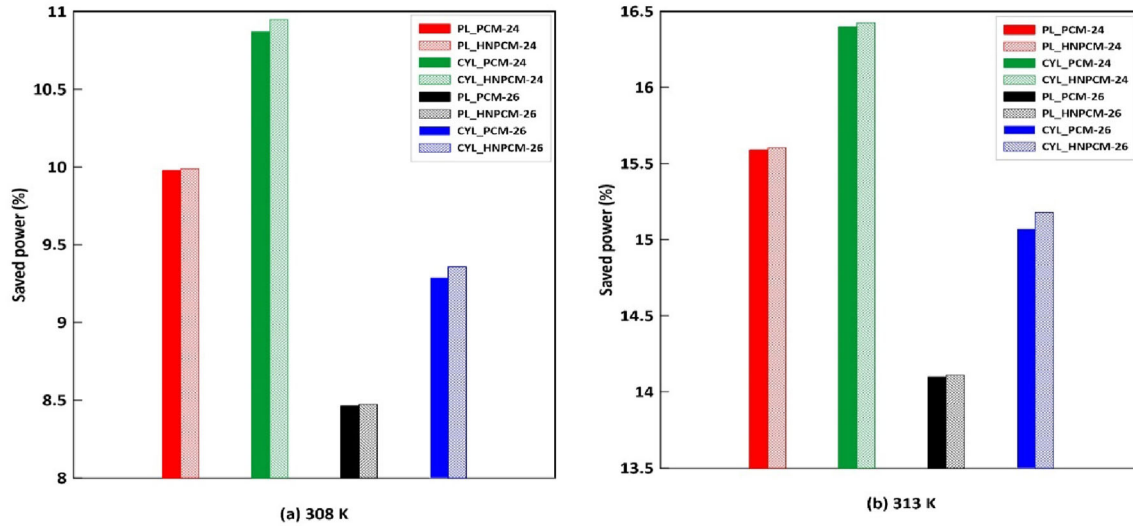


Fig. 9. Percentage AC saved power for 2 working hours at inflow air temperatures of (a) 308 K and (b) 313 K.

enhanced unit's COP by about 70% for CYL\_PCM-24. In addition, the CYL\_HNPCM-24 configuration starts with the highest COP, while the PL\_PCM-26 configuration starts with the lowest COP. After a certain amount of time, the trend is reversed; the CYL\_HNPCM-24 configuration has the lowest COP because it melts faster than all the other cases.

Moreover, utilizing PCM with a higher MT (PCM-26) decreases the percentage gain in COP of both configurations in the beginning period compared to PCM-24. For example, at an inflow air temperature of 313 K, the maximum increased percentage of COP at the start is about 24%, 22%, 20%, and 18% for CYL\_PCM-24, CYL\_PCM-26, PL\_PCM-24, and PL\_PCM-26 configurations, respectively. After 3 h, the previous results turned into 1%, 2%, 12.7%, and 13%, respectively, as shown in Fig. 8b. Nevertheless, the inclusion of hybrid nanoparticles into PCM increases the COP of the enhanced unit for a short running time in all studied cases. However, this effect is reversed when the unit is used for a long time (Fig. 8).

### Power Saving

It is essential to determine how much electricity this AC storage energy solution saves over a regular AC unit. Based on the COP, both improved and regular units' power consumption is calculated using Eq. 13 per ton refrigerant. Figure 9 depicts the modified unit's saved power compared to the traditional unit for both configurations at different inflow air temperatures (308 K and 313 K) and PCM types for 2 h of AC operation (minimum hottest ambient hours required for AC running) while Fig. 10 demonstrates the same outcomes for 8 h of AC running (approximately maximum total daytime). Also, the effect of adding hybrid nanoparticles to PCM on the power saving of the modified

AC unit is presented. According to the outcomes, the power usage of the modified unit is lower than that of the regular unit in all evaluated configurations and cases during PCM cooling time. In addition, the total power-saving rises with increasing ambient inlet temperature.

It is clear from the figures that for low running hours of AC unit, CYL\_PCM-24 configurations achieve the maximum saving power, followed by PL\_PCM-24 and CYL\_PCM-26 configurations, while PL\_PCM-26 configurations have the minimum saving power. The maximum power saving between all studied cases for short-term running is 10.95% and 16.4% for CYL\_HNPCM-24 configuration at 308 K and 313 K inflow temperatures, respectively. However, for higher running hours of the AC, the PL\_PCM-26 configurations have the highest power saving, and CYL\_PCM-24 records the lowest power saving. As given in Fig. 10, the maximum power saving is 5.51% and 6.4% for the PL\_PCM-26 configuration at inflow temperatures of 308 K and 313 K, respectively. As discussed previously, nanoparticles mixed with PCM have a short-term positive influence on the performance of the modified AC unit. However, the effect is negative for a long running time, as seen in Fig. 10. Therefore, it can be concluded that the CYL with HNPCM-24 configuration is more effective for applications requiring a short working period, whereas PL with PCM-26 configuration is the best choice for a long working period of the AC unit.

Eventually, a brief comparison is conducted between the current work and other published works with similar concepts, the idea of integrating a PCM system into an AC unit, as shown in Table VI in terms of power savings, and the PCM used. As shown, the PCM capsulated in cylinders and



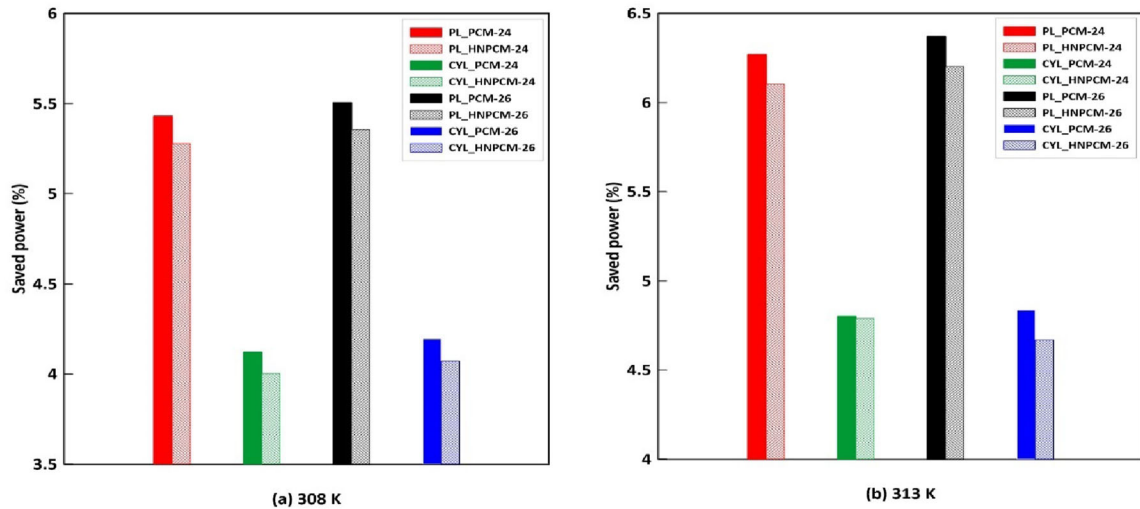


Fig. 10. Percentage AC saved power for 8 working hours at inflow temperatures of (a) 308 K and (b) 313 K.

**Table VI. A comparison of the current study outcomes with other previous studies**

Study	Concept	PCM used	Main outcomes
Said et al. <sup>2</sup>	Coupling a PCM plate heat exchanger to an AC unit's condenser	Rubitherm (SP24E)	Maximum power savings reached 6.7% and 5.4% for inlet temperatures of 40°C and 35°C
Said et al. <sup>27</sup>	Coupling different PCMs types with an AC unit's condenser	Rubitherm (SP24E) Rubitherm (SP26E) Rubitherm (SP29Eu)	At 35°C inlet air temperature, the maximum power savings reached 4.4%, 4.3%, and 4.05% for PCM 24E, PCM 26E, and PCM 29Eu
Chaiyat <sup>46</sup>	Integrating a PCM bed before the evaporator	Rubitherm (RT20)	Decreasing power consumption by 3.09 kW h/day
Hoseini et al. <sup>26</sup>	Utilizing a PCM tank with an AC system to shift the peak load	Rubitherm (RT3HC)	Power consumption reduction by 7.58%
Current	Incorporating different PCM configurations (plates and cylinders) and types into the AC condenser	Rubitherm (SP24E) Rubitherm (SP26E) PCM-nanoparticles mixture	The maximum power saving was 10.94% and 16.4% for cylinder configuration for inlet temperatures of 35°C and 40°C

integrated into the AC condenser records a higher power saving compared to other given studies.

**PCM Charging**

Recharging the PCM (solidification) is necessary since the PCM dissipates all its cold energy into the air throughout the daytime. The low night temperatures allow for this solidification process to be carried out. As a result, it is essential to ascertain how long it takes for liquid PCM to solidify. Figure 11 presents the time variation of the liquid fraction of tested PCMs during the charging process for both configurations at an inflow air temperature of 295 K (the average ambient night temperature for hot climate conditions). As observed, the

charging rate is significantly affected by the PCM melting temperature and configuration. To clarify, increasing the MT of PCM from 297 K to 299 K decreases PCM's full solidification time (FST) by around 40% for both configurations. This is because the temperature difference between night temperature and PCM with higher MT is greater, contrary to the melting process. Moreover, the FST of the cylinder structure is greater than that of the plate structure by around 25%. The CYL\_HNPCM-26 configuration achieves the fastest FST, while the PL\_PCM-24 configuration has the slowest FST. This would be related to the same reasons for the discharging process, as cylinders have a higher heat transfer flux. Furthermore, the FST differs slightly

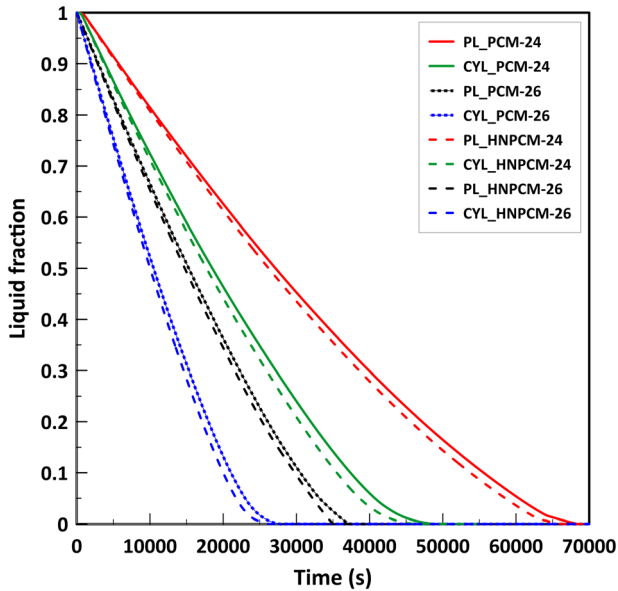


Fig. 11. Variation of liquid fraction during PCM charging with time.

between PCM with and without hybrid nanoparticle configurations.

On the other hand, if the FMT from Fig. 6 is compared to the FST from Fig. 11, it is clear that the FST is longer than the FMT. This is because the temperature difference between the MT of PCM and the ambient air during the day is larger than at night. Subsequently, as previously indicated, the PCM configuration and MT are the most appropriate and cost-effective parameters to govern the melting and solidification period.

## CONCLUSION

AC system performance is theoretically done using two PCM design configurations (cylinders and plates). In addition, the effect of inflow air temperature and PCM melting temperature on the air-PCM heat exchanger is studied. Furthermore, hybrid nanoparticles are added to the PCM to examine their effect on the AC performance. PCM melting rate, exit air temperature from the heat exchanger, charging process, COP, and AC unit saving power are all reported as a result of the abovementioned parameters. The results conclude that raising the inflow air temperature of the air-PCM heat exchanger increases the temperature difference between the inlet and outlet, COP, and power saving of the AC unit, but the discharging time decreases while increasing the melting temperature of PCM from 297 K to 299 K causes the melting time to be longer but shortens the time of solidification. For the short-term operation of the AC unit with a high cooling load, cylinder configuration with low PCM MT and HN is convenient. Plate layout with a high PCM MT is best suited for long-term operation with a high cooling load; the

challenge is the lengthy solidification period. The solidification time of cylinder configuration is lower than that of plate configuration by approximately 25%. Using hybrid nanoparticles with PCMs enhances PCM's thermal properties but slightly impacts the AC performance. This modified AC unit's highest percentage of saved power is about 10.95% and 16.4% for CYL\_HNPCM-24 for 2 running hours and is about 5.51% and 6.4% for the PL\_PCM-26 configuration at inflow temperatures of 308 K and 313 K, respectively, for 8 running hours of the unit. Generally, the results propose that PCM mixed with nanoparticles and encased in cylinders incorporated into the AC system has a considerable improvement in the charging and discharging process and can create meaningful power saving of AC throughout the discharging process, all while being easier to process and less expensive to make for industry sectors and residences. Consequently, PCM cylinders are anticipated to be widely used to improve latent heat storage and power consumption in AC systems. So, based on these results, a great value of energy can be saved, and hence a large amount of CO<sub>2</sub> reduction can be obtained.

## ACKNOWLEDGEMENTS

The authors acknowledge the Mission Department of the Ministry of Higher Education (MOHE) of Egypt for providing a scholarship to conduct this study as well as the Japan International Cooperation Agency (JICA) for offering some of the facilities, tools, and equipment and the Science, Technology & Innovation Funding (STDF) department which is sponsoring the research work to conduct this study under Project No. 43566.

## FUNDING

Open access funding provided by The Science, Technology & Innovation Funding Authority (STDF) in cooperation with The Egyptian Knowledge Bank (EKB).

## CONFLICT OF INTEREST

On behalf of all authors, the corresponding author states that there is no conflict of interest.

## OPEN ACCESS

This article is licensed under a Creative Commons Attribution 4.0 International License, which permits use, sharing, adaptation, distribution and reproduction in any medium or format, as long as you give appropriate credit to the original author(s) and the source, provide a link to the Creative Commons licence, and indicate if changes were made. The images or other third party material in this article are included in the article's Creative Commons licence, unless indicated otherwise in a credit line to the material. If material is not included in the article's Creative Commons licence and your intended use is not permitted by statutory

regulation or exceeds the permitted use, you will need to obtain permission directly from the copyright holder. To view a copy of this licence, visit <http://creativecommons.org/licenses/by/4.0/>.

## REFERENCES

1. A.A. Al-Abidi, S. Bin Mat, K. Sopian, M.Y. Sulaiman, C.H. Lim, and A. Th, *Renew. Sustain. Energy Rev.* 16, 5802 (2012).
2. M.A. Said and H. Hassan, *Appl. Energy* 230, 1380 (2018).
3. S.K. Wang and S.K. Wang, *Handbook of Air Conditioning and Refrigeration* (McGraw-Hill, New York, 2000).
4. T.T. Chow, Z. Lin, and X.Y. Yang, *Appl. Therm. Eng.* 22, 1431 (2002).
5. A.T. Muzhanje, M.A. Hassan, S. Ookawara, and H. Hassan, *J. Energy Storage* 51, 104353 (2022).
6. C. Aprea and A. Maiorino, *Appl. Therm. Eng.* 27, 2592 (2007).
7. A. Avara and E. Daneshgar, *Energy Build.* 40, 1268 (2008).
8. L.D. Abishai, M.E. Surejlal, S.S. Harish, and S.S. Prabu, *Materials Today: Proceedings* (Elsevier, Amsterdam, 2021), pp 2671–2677.
9. M. Bruelisauer, F. Meggers, E. Saber, C. Li, and H. Leibundgut, *Energy Build.* 71, 28 (2014).
10. M. Saffari, A. de Gracia, C. Fernández, and L.F. Cabeza, *Appl. Energy* 202, 420 (2017).
11. M.S. Yousef, H. Hassan, S. Kodama, and H. Sekiguchi, *Energy Procedia* 156, 100 (2019).
12. X.Q. Zhai, X.L. Wang, T. Wang, and R.Z. Wang, *Renew. Sustain. Energy Rev.* 22, 108 (2013).
13. S.F. Li, Z. Liu, and X.J. Wang, *Appl. Energy* 255, 113667 (2019).
14. V. Vakiloroyaya, B. Samali, A. Fakhar, and K. Pishghadam, *Energy Convers. Manag.* 77, 738 (2014).
15. A.M. Khudhair and M.M. Farid, *Energy Convers. Manag.* 45, 263 (2004).
16. B. Zalba, J.M. Marín, L.F. Cabeza, and H. Mehling, *Appl. Therm. Eng.* 23, 251 (2003).
17. E. Osterman, V.V. Tyagi, V. Butala, N.A. Rahim, and U. Stritih, *Energy Build.* 49, 37 (2012).
18. F. Souayfane, F. Fardoun, and P.H. Biwole, *Energy Build.* 129, 396 (2016).
19. J. Jeon, J.-H. Lee, J. Seo, S.-G. Jeong, and S. Kim, *J. Therm. Anal. Calorim.* 111, 279 (2013).
20. E. Kirilovs, I. Zotova, S. Kukle, and K. Pugovics, *J. Energy Syst.* 5, 1 (2021).
21. H. Selvnes, Y. Allouche, R.I. Manescu, and A. Hafner, *Therm. Sci. Eng. Prog.* 22, 100807 (2021).
22. K. Panchabikesan, A.A.R. Vincent, Y. Ding, and V. Ramalingam, *Energy* 144, 443 (2018).
23. M.A. Said and H. Hassan, *Energy Build.* 173, 353 (2018).
24. M.N. Ajour, M.J. Abdual, F.A. Hariri, N.H. Abu-Hamdeh, and A. Karimipour, *J. Build. Eng.* 57, 104915 (2022).
25. T. Hai, S.M. Sajadi, J.M. Zain, A.S. El-Shafay, and M. Sharifpur, *J. Build. Eng.* 49, 104079 (2022).
26. M. Hoseini Rahdar, A. Emamzadeh, and A. Ataei, *Appl. Therm. Eng.* 96, 391 (2016).
27. M.A. Said and H. Hassan, *Energy Build.* 202, 109353 (2019).
28. B. Huang, Z. Zheng, G. Lu, and X. Zhai, *Energy Build.* 259, 111871 (2022).
29. A. Takudzwa Muzhanje, M.A. Hassan, and H. Hassan, *Appl. Therm. Eng.* 214, 118832 (2022).
30. R. Elbahjaoui and H. El Qarnia, *Energy Build.* 153, 1 (2017).
31. N.S. Dhaidan, J.M. Khodadadi, T.A. Al-Hattab, and S.M. Al-Mashat, *Int. J. Heat Mass Transf.* 66, 672 (2013).
32. R. Parameshwaran and S. Kalaiselvam, *Energy Build.* 69, 202 (2014).
33. K. Kant, A. Shukla, A. Sharma, and P. Henry Biwole, *Sol. Energy* 146, 453 (2017).
34. A.H.A. Al-Waeli, K. Sopian, M.T. Chaichan, H.A. Kazem, A. Ibrahim, S. Mat, and M.H. Ruslan, *Energy Convers. Manag.* 151, 693 (2017).
35. F. Bahiraei, A. Fartaj, and G.A. Nazri, *Energy Convers. Manag.* 153, 115 (2017).
36. X. Sun, L. Liu, Y. Mo, J. Li, and C. Li, *Appl. Therm. Eng.* 181, 115992 (2020).
37. L. Yang, J. Huang, and F. Zhou, *Energy Convers. Manag.* 214, 112876 (2020).
38. K. Hosseinzadeh, E. Montazer, M.B. Shafii, and A.R.D. Ganji, *J. Energy Storage* 34, 102177 (2021).
39. M.A. Said and H. Hassan, *Energy Convers. Manag.* 171, 903 (2018).
40. A.A.R. Darzi, S.M. Moosania, F.L. Tan, and M. Farhadi, *Int. Commun. Heat Mass Transf.* 48, 155 (2013).
41. M.G. Gado, S. Ookawara, S. Nada, and H. Hassan, *Int. J. Refrig.* 142, 66 (2022).
42. R. Gad, H. Mahmoud, S. Ookawara, and H. Hassan, *J. Clean. Prod.* 364, 132489 (2022).
43. E.M. Barreira, C.O.R. Negrão, and C.J.L. Hermes, *Appl. Therm. Eng.* 50, 629 (2013).
44. S.A. Nada and M.A. Said, *Appl. Therm. Eng.* 123, 874 (2017).
45. M.A. Said and H. Hassan, *J. Energy Storage* 36, 102400 (2021).
46. N. Chaiyat, *Energy Convers. Manag.* 94, 150 (2015).

**Publisher's Note** Springer Nature remains neutral with regard to jurisdictional claims in published maps and institutional affiliations.